ASPECTS REGARDING THE HOT FRACTURE BEHAVIOR OF 42CrMo4 ALLOY

M. POP*, D. FRUNZA, F. POPA, A. NEAG

Technical University, Faculty of Materials Engineering and Environment, B-dul Muncii 103–105, Cluj-Napoca, Romania
*Corresponding author: Mariana.Pop@ipm.utcluj.ro

Received November 10, 2016

Abstract. The hot tensile deformation behavior of 42CrMo4 steel are studied by uniaxial tensile tests with the temperature range of 750–1000° C and strain rate range of 0.1–0.005s^{-1} . The effects of hot forming process parameters (strain rate and deformation temperature) on the elongation to fracture and fracture characteristics are analyzed. The flow behavior is significantly affected by the deformation temperature, strain and strain rate. The flow stress decreases with the increase of deformation temperature and the decrease of strain rate. The flow stress firstly increases to a peak value and then decreases, showing a dynamic flow softening. This is mainly due to the dynamic recrystallization and material damage during the hot tensile deformation. The simulation results confirm the suitability of the current finite element software for modeling the three-dimensional hot tension of 42CrMo4 steel.

Key words: 42CrMo4 steel, flow stress, temperature, strain rate, ductile fracture, numerical simulation.

1. INTRODUCTION

In industrial forming processes, the metals and alloys are subjected to complex time, strain, strain rate, and temperature histories. On the one hand, a given combination of thermo-mechanical parameters yields a particular metallurgical phenomenon (microstructural evolution); on the other hand, microstructural changes of the metal during the hot forming process in turn affect the mechanical characteristics of the metal such as the flow stress, and hence influence the forming process [2, 7, 13, 15].

Hot working is often defined as working above the recrystallization temperature so that the work metal recrystallizes as it deforms. However, this is an oversimplified view. The strain rates of many metalworking processes are so high that there is not time for recrystallization to occur during deformation. Rather, recrystallization may occur in the time period between repeated operations, as in forging and multiple-stand rolling, or after the deformation is complete, while the material is cooling to room temperature.

The high temperature does, however, lower the flow stress whether recrystallization occurs during the deformation or not. Furthermore, the resultant product is in an annealed state [8]. Material flow behavior during hot formation process is often complex. The *work hardening* (WH), *dynamic recovery* (DRV) and *dynamic recrystallization* (DRX) often occur in the metals and alloys with low stacking fault energy during the hot deformation [9, 17, 22]. Especially, the effects of DRX behavior on the flow stress and microstructures are significant for the metals and alloys. Therefore, understandings of the relationship between the thermo-mechanical parameters and DRX behavior of metals and alloys is of great importance for designers of metal forming processes (hot rolling, forging and extrusion). It is well known that the *dynamic recrystallization* (DRX) can refine the grain during the hot deformation. As an important softening and grain refinement mechanism, the DRX has a great significance for the control of microstructures and the improvement of mechanical properties [9]. 42CrMo4 is a low-alloy steel widely used in various applications such as automotive driving elements (steering components, crankshafts), bolted assemblies, forged parts welded components, armour materials and among other applications [1, 6, 11, 12, 25]. It is characterized by a high strength, an interesting fatigue behavior and good machinability [23, 27]. Despite that 42CrMo4 steel material properties of are well documented, there is still an interest in studying the mechanical properties of such material [14, 20, 21, 27]. 42CrMo4 steel contains chromium and molybdenum as alloying elements and may be heat treated over a wide range to give the combined advantages of proper hardness, strength and ductility. In conditions where localized hardness may be required, this steel is readily flame or induction hardened. In the past, many investigations have been carried out on the behavior of 42CrMo steel [16]. Despite large amount of efforts invested into the behaviors of 42CrMo steel, the effects of hot forming processing parameters on the strain/stress distribution and microstructural evolution of hot deformed 42CrMo steel need to be further investigated to study the workability and optimize the hot forming processing parameters.

The correlation between the flow stress, strain rate and deformation temperature during hot deformation can be expressed by the Zener–Hollomon parameter (Z), defined by the equation [28]:

$$z = \dot{\varepsilon}\exp(\frac{Q}{RT}), \tag{1}$$

where: $\dot{\varepsilon}$ is the strain rate, Q is the activation energy for deformation, R is the gas constant, and T is the deformation temperature (K).

The workability of metal plays a major role for judging whether the metal will be manufactured successfully or caused by ductile fracture in the forming process. And the ductile fracture is usually the main reason for the failed workpiece. So the prediction of the fracture initiation is an important item in the forming category. Based on various hypotheses, many criteria for ductile fracture have been proposed empirically as well as theoretically [4, 5, 26]. Most of these criteria relate to the critical plastic work *per unit* of volume; such as the Freudenthal criterion, Cockcroft-Latham criterion, normalized Cockcroft-Latham criterion [24].

All the integrated stress–strain criteria based on empirical and semiempirical approach are versions of Freudenthal's critical plastic work *per unit* of volume [24]:

$$\int_0^{\overline{\varepsilon_f}} \overline{\sigma}\, d\,\overline{\varepsilon} = C_1\,, \tag{2}$$

where: $\overline{\sigma}$ is the effective stress, $d\,\overline{\varepsilon}$ is effective strain increment and $\overline{\varepsilon_f}$ is the effective strain at fracture (Freudenthal, 1950). C_i, where i: 1, 2, ... are critical values, calculated by using these criteria.

In the present study, uniaxial tensile tests were conducted on a 42CrMo4 alloy under wide ranges of deformation temperature and strain rate. Effects of the deformation parameters on the flow behavior, and fracture characteristics are studied. Scanning electron microscopy is used together with fractography to characterise the microstructure of the alloys and to study the damage and fracture mechanisms.

2. EXPERIMENTAL PROCEDURE

The 42CrMo4 high-strength steel employed in the present investigation was provided in the form of bar with the diameter of 20 mm. Cylindrical tensile specimens with 30 mm in gauge length and 5 mm in diameter were machined. Nominal chemical composition (in weight %) of 42CrMo4 alloy, which was received as extruded bar is: 0.42% C; 0.25% Si; 0.75% Mn; 0.22% Mo; 1.1% Cr; <0.035% S; <0.035% P. Then the tension tests were carried out at four different temperatures of 700° C, 800° C, 900° C and 1000° C and four different strain rates of 0.005 s^{-1}, 0.02 s^{-1} and 0.1 s^{-1}.

The equipment used for the tensile tests is represented in Fig. 1. The dimensions of the tensile specimen are illustrated in Fig. 2.

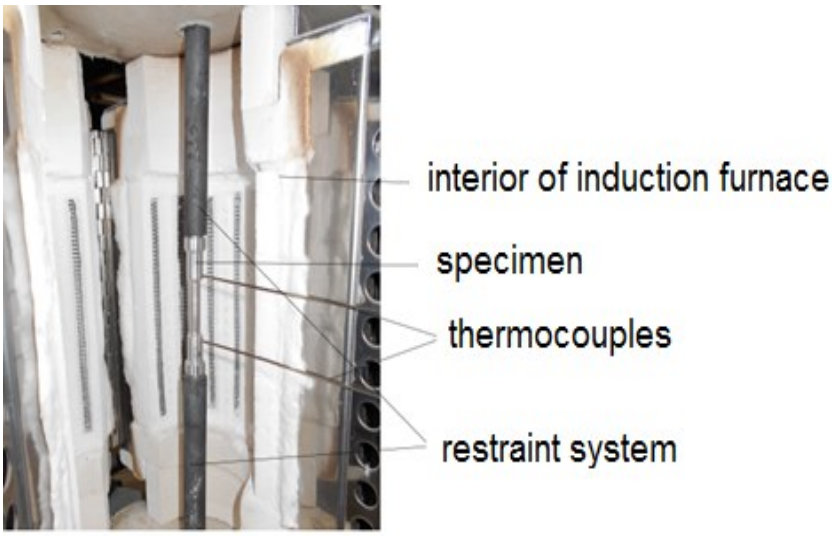

Fig. 1 – The specimen in the induction heating furnace.

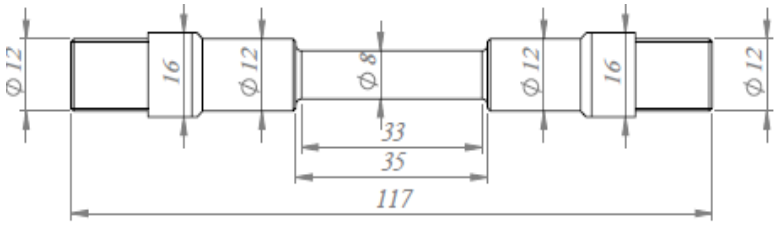

Fig. 2 – Dimensions of the tensile specimen.

During the tension process, the variations of stress and strain were monitored continuously by a personal computer equipped with an automatic data acquisition system. The specimens were firstly heated to the target deformation temperature, held for 15 minutes to eliminate the thermal gradient. Then, the specimens were stretched at the selected constant temperatures and strain rates. This was followed by quenching the specimens in water just after straining. The elongation-to-failure was measured from the gauge length of the fractured specimen.

3. RESULTS AND DISCUSSIONS

The typical tensile stress-true strain curves obtained from tensile tests at different strain rates are presented in Fig. 3.

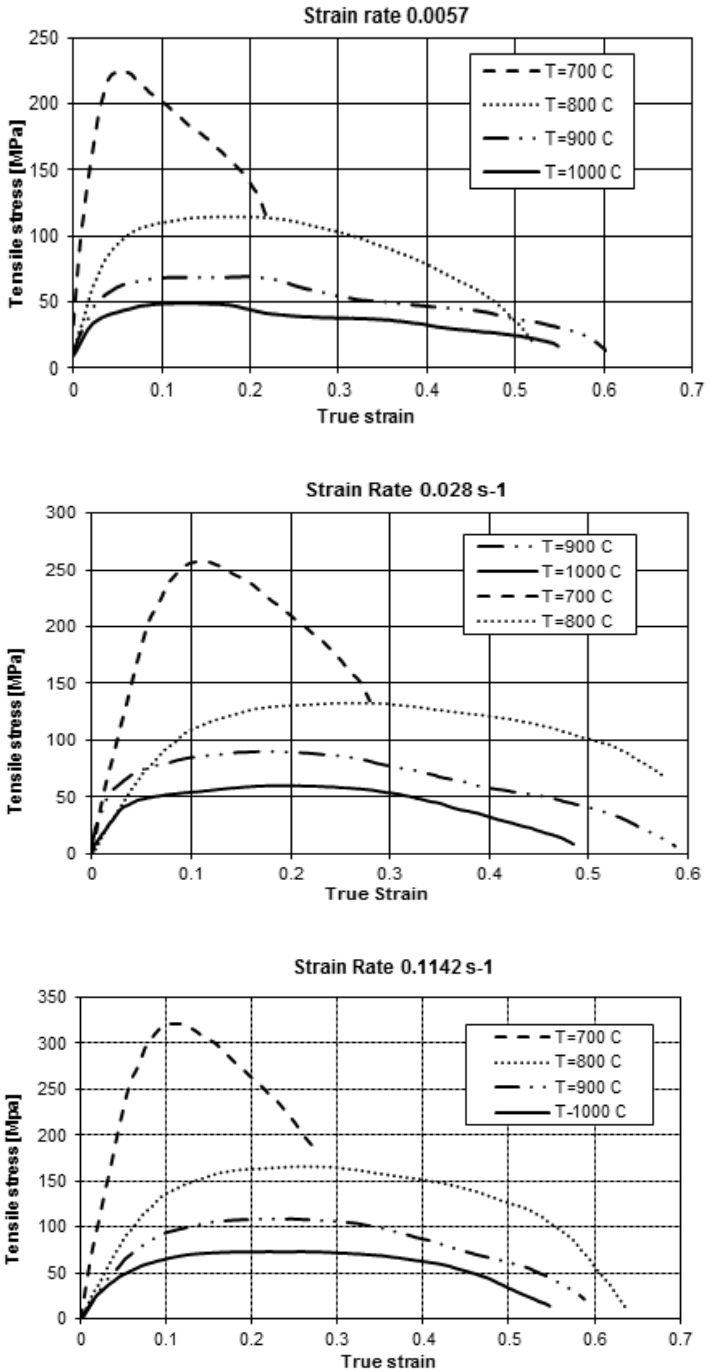

Fig. 3 – True stress-true strain curves.

The tested specimens after fracture are presented in Figure 4.

Fig. 4 – Specimens tested in tension.
a) Initial specimen; b) $T = 1000^{o}$ C, $\dot{\varepsilon} = 0.11 s^{-1}$; c) $T = 900^{o}$ C, $\dot{\varepsilon} = 0.11\ s^{-1}$; d) $T = 800^{o}$ C, $\dot{\varepsilon} = 0.11 s^{-1}$; e) $T = 700^{o}$ C, $\dot{\varepsilon} = 0.11\ s^{-1}$.

The Cauchy stress and the real strain were calculated as:

$$\sigma = \frac{F}{A} \tag{3}$$

and

$$\delta = \ln \frac{A_0}{A} \tag{4}$$

where F is the force, A_0 is the initial cross-section area, and A is the final cross-section area of the specimen.

For the strain and strain rate sensitive materials, the hot deformation characteristics can usually be described by the following power law equation [9].

$$\sigma = K\epsilon^n \dot{\epsilon}^m, \tag{5}$$

where: K is material constant, n is strain hardening exponent, m is strain rate sensitivity coefficient.

The results show that the deformation of the specimen is inhomogeneous and the degree of the deformation inhomogeneity decreases with the increase of strain rates. The distribution of the effective stress in the specimen is also inhomogeneous, and the locus of the maximum effective stress changes with the variations of strain rates.

As is evident, the flow stress characteristics are significantly dependent on the temperature and strain rate. It can be seen that all of the flow curves exhibit initial strain hardening and softening after the peak stress. Such behaviour of flow

stress is the typical feature indicating that the dynamic recrystallization (DRX) occurs during the hot deformation. The flow softening tendency becomes greater with an increase in the deformation temperature and a decrease in the strain rate. This behaviour is because the higher temperature can offer higher mobility to the dislocations and grain boundaries and a longer deformation time (in the case of the low strain rates) for the dislocation annihilation, nucleation and growth of new grains [3].

The flow stress firstly increases to a peak value, which is associated with the combined effects of work hardening and dynamic recovery. When the balance between the work hardening and dynamic recovery softening is achieved, the flow curves show a long steady stress stage, in which the flow stress nearly remains constant with the further straining. Then, the flow stress decreases monotonously till fracture with the increase of strain. The decrease in flow stress at high temperatures permits lower tool forces and, consequently, equipment size and power requirements. From the true stress-strain curves, it can be seen that the stress evolution with strain exhibits three distinct stages. At the first stage where work hardening predominates, flow stress exhibits a rapid increase. At the second stage, flow stress exhibits a smaller increase until reaching a peak value. This phenomenon shows that the thermal softening due to dynamic recrystallization and dynamic recovery becomes more predominant. At the third stage, flow stress decrease gradually to a steady state with dynamic recrystallization softening.

With the increase of deformation temperature or the decrease of strain rate, the work hardening and steady stress stages are shortened, while the flow softening stage is prolonged [18]. Researches show that the strain rate sensitivity influences the necking or stain-localization in metals or alloys during hot tensile deformation [10].

To examine the microstructure evolution and the fracture mechanisms, the specimens were sliced and the cross section in the longitudinal direction of the failed tensile specimens was polished and investigated for the various alloys in the scanning electron microscope.

Typical fracture surfaces of the tensile test specimens in different conditions of deformation are shown in Fig. 5.

In all cases the fracture mode is cup-and-cone. The cross-sectional area at fracture decreases with increasing deformation temperature due to the increase in ductility.

Figure 6 shows the sectional fracture morphologies of the failure specimens under the strain rate of 0.1 s^{-1} and deformation temperatures of 700, 800 and 900° C. The fracture surfaces are all covered with typical equiaxed dimples. Failure occurs by the formation and coalescence of the microvoids.

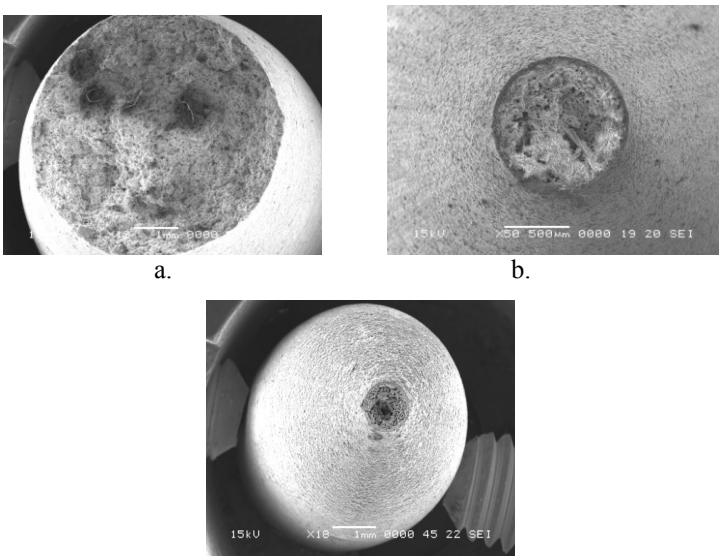

Fig. 5 – Scanning electron micrographs of fracture surface
a) $T = 700^{o}$ C, $\dot{\varepsilon} = 0.11\ s^{-1}$; b) $T = 800^{o}$ C, $\dot{\varepsilon} = 0.11\ s^{-1}$; c) $T = 900^{o}$ C, $\dot{\varepsilon} = 0.11\ s^{-1}$.

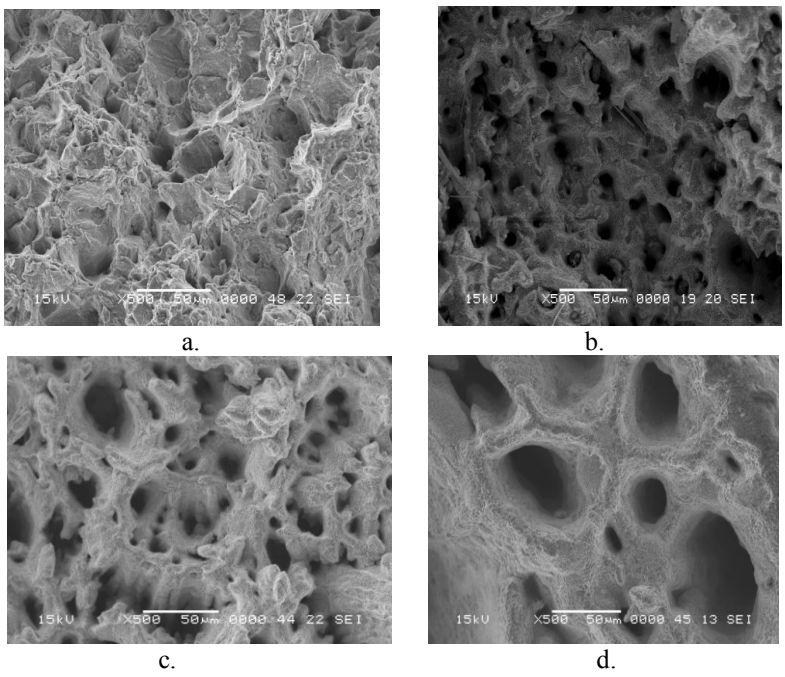

Fig. 6 – The SEM images of tensile fracture appearance: a) $T = 700^{o}$ C, $\dot{\varepsilon} = 0.1\ s^{-1}$; b) $T = 800^{o}$ C, $\dot{\varepsilon} = 0.1\ s^{-1}$; c) $T = 900^{o}$ C, $\dot{\varepsilon} = 0.1\ s^{-1}$; d) $T = 1000^{o}$ C, $\dot{\varepsilon} = 0.1 s^{-1}$.

The size of the microvoids decreases with decreasing of the deformation temperature. Due to the fact that the internal necking is hard to occur under relatively low deformation temperature, the deformation process tends to generate more microscopic dimples. Cavity nucleation is a continuous process during large plastic deformation process [9]. Cavities tend to nucleate in the phase boundary between the matrix and the second phase particles or around large nonmetallic inclusions. At the final deformation stage, the growth and coalescence of cavities perpendicular to the loading axis causes the decrease of the effective cross section of specimens, and thus causes rapid fracture of material. Generally, the nucleation, growth and coalescence of cavities will cause the dynamic softening and deteriorate the deformation properties of materials. Furthermore, the damage degree induced by cavities becomes more and more serious with the increase of the deformation temperature. Also the strain to failure decreases with increasing yield stress.

4. SIMULATION DETAILS

A simulation of the extrusion process was performed using the finite element software. Forge is a commercial software developed at CEMEF, École des Mines de Paris and is used for the analysis of plastic deformation processes. The program is based on the finite element method for cold and hot metal forming. It enables the thermo-mechanical simulation of the plastic deformation processes of metals in an axisymmetric, homogeneous and isotropic state of deformation and obeys the von Mises criterion. This was achieved by constructing an accurate three dimensional CAD model of the process. The model was meshed with appropriate elements and material properties and boundary conditions were added. The geometries of the billet and tools were generated in SolidWorks and the meshes within their space domains in FORGE 3D. The physical properties of the 42CrMo4 alloy used in the computer simulation are given in Table 2.

Table 2

Properties	Material 42CrMo4
Density (kg/m^3)	7800
Heat capacity (J/kgK)	460
Thermal conductivity (W/mK)	35

The process parameters used in the simulations are given in Table 3.

Table 3

Billet length [mm]	36
Billet diameter [mm]	8
Billet temperature [°C]	700, 800, 900, 1000
Ram speed [m/s]	0.2; 1; 4
Friction factor at the workpiece–die interface	0.3

The billet was considered thermo-viscoplastic, while the tools rigid, and both of these material models neglected the elastic deformation. The shear-type friction conditions at the workpiece and tooling interfaces were imposed as part of the boundary conditions. The friction factor, according to Tresca friction law, at the billet-die interfaces were assumed to be 0.3.

In Fig. 7a,b are presented the experimental and simulated stress-strain curves that were obtained for different strain rates.

Figures 8 and 9 present the distribution of the von Mises effective stress inside the billet and the damage value obtained with the normalized C & L ductile fracture criterion, at a particular stage of traction determined by the simulation model.

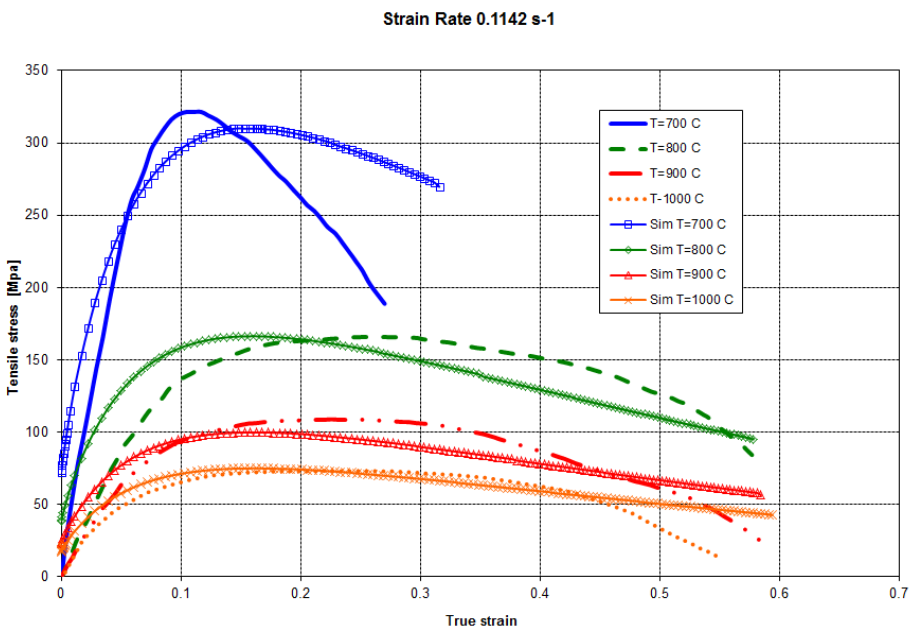

Fig. 7a – Experimental and simulated stress-strain curves for strain rate 0.1142 s^{-1}.

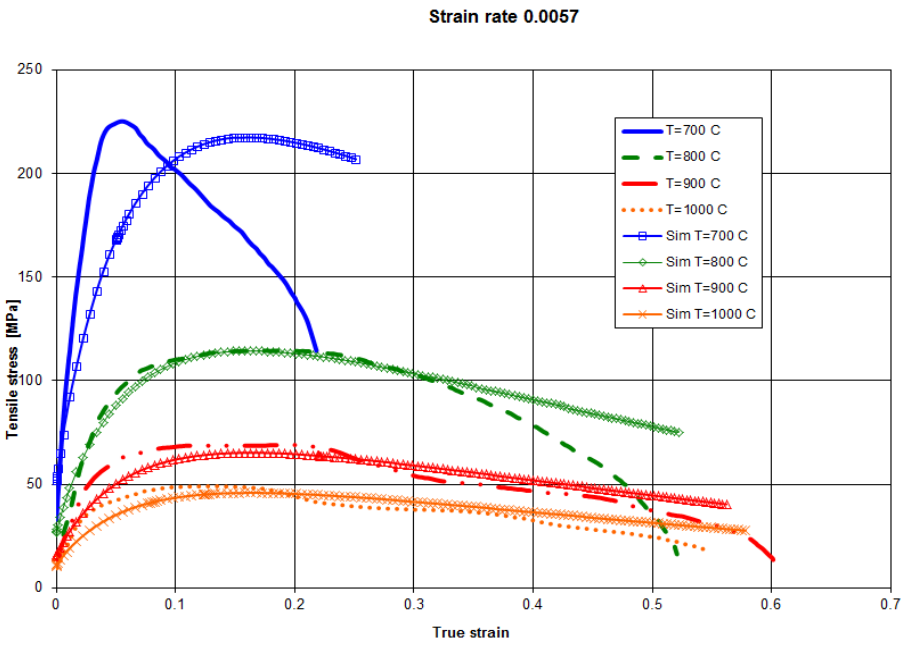

Fig. 7b – Experimental and simulated stress-strain curves.

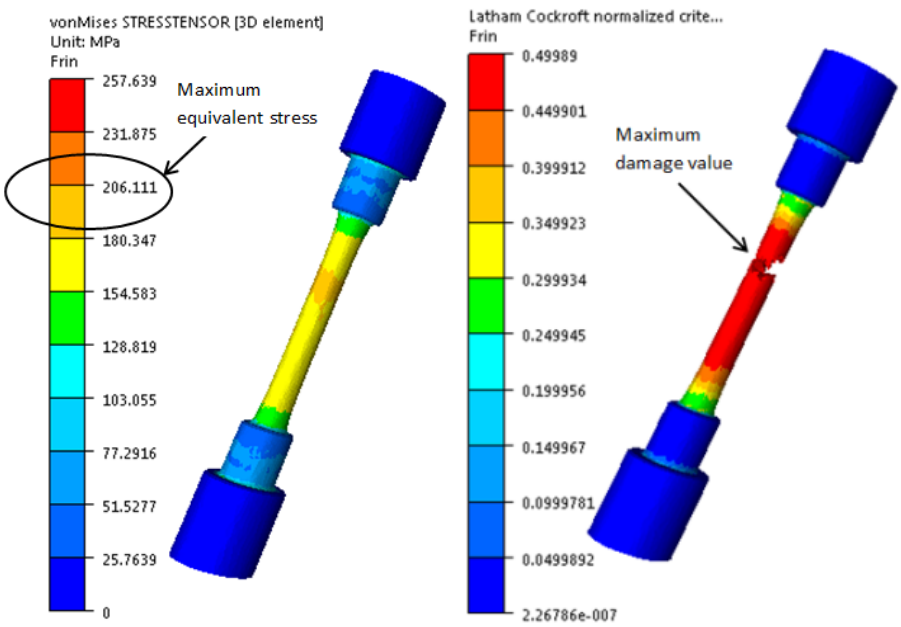

Fig. 8 – von Mises effective stress and damage value distribution at $T = 700^{o}$ C, $\dot{\varepsilon} = 0.005$ s^{-1}.

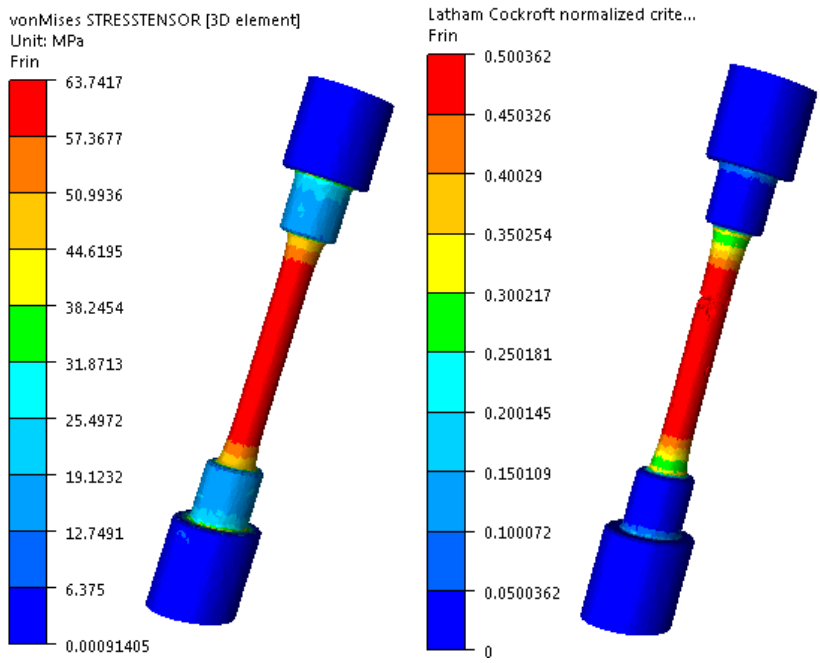

Fig. 9 – von Mises effective stress and damage value distribution at $T = 900^{o}$ C, $\dot{\varepsilon} = 0.005$ s^{-1}.

Comparisons were made for the experimental with simulated true stress-true strain curves. It is found that for evaluated conditions, experimental curves have the same shape as simulated ones. The average error between the experimental and simulated curves is below 10%.

The close agreement between the simulation and experimental results confirms the validity of the tension tests for evaluated conditions.

5. CONCLUSIONS

The hot tensile deformation behaviors of 42CrMo4 steel are investigated over wide ranges of deformation temperature and strain rate. The effects of deformation parameters on the flow behavior and fracture characteristics are studied. Some important conclusions can be made as follows: the flow behaviors are significantly affected by the deformation temperature and strain rate; the flow curves are composed of three distinct stages, work hardening stage, steady stress stage and flow softening stage; dynamic recrystallization occurs during the tensile deformation process; the refining of microstructure caused by DRX improves the plastic deformation capacity of the material and increases the elongation to fracture; ductile fracture failure occurs, which result from the effects of localized

necking and microvoid coalescence under all the deformation conditions; the nucleation, growth and coalescence of cavity occur during the hot plastic deformation, and the material damage degree induced by cavities increases with the increase of deformation temperature.

REFERENCES

1. N. Arivazhagan, S. Singh, S. Prakash, GM. Reddy, *Int. J. Adv. Manuf. Technol*. **39**, 679–689 (2008).
2. S. Bouvier, J.L. Alves, M.C. Oliveira, L.F. Menezes, Comput. Mater. Sci. **32**, 301 (2005).
3. A.Yu. Churyumov, M.G. Khomutov, A.N. Solonin, A.V. Pozdniakov, T.A. Churyumova, B.F. Minyaylo, Materials and Design **74**, 44–54 (2015).
4. S.E. Clift, P.Hartley, E.N.Sturgess, G.W.Rowe, Int. J. of Mechanical Sciences. **32**(1), 1–17(1990).
5. M.G. Cockcroft, D.J. Latham, Journal of the Institute of Metals **96**, 33–39 (1968).
6. Demir T, Ubeyli M, Yildrim RO., Materials Design **29**, 2009–16 (2008).
7. R. Ebrahimi, S.H. Zahiri, A. Najafizadeh, J. Mater. Process. Technol. **171**, 301 (2006).
8. W. Hosford, R. Caddell, Metal Forming, Mechanics and Metallurgy, Prentice Hall (1993).
9. Huang Yuan-Chun, Y.C. Lin, Jiao Deng, Ge Liu, Ming-Song Chen, Materials and Design, **53**, 349–356 (2014).
10. J.W. Hutchinson, K.W.Neale, Acta Metallurgica, **25**,839–846 (1977).
11. E.Ilhan, F.Findik, S.Aslanlar, Materials Design **24**:503–507 (2003).
12. E.Karadeniz, Materials Design **29**,251–6 (2008).
13. B.H. Lee, N.S. Reddy, J.T. Yeom, C.S. Lee, J. Mater. Process. Technol. **187–188**, 766 (2007)**.**
14. Leslie WC., The physical metallurgy of steels. New York: McGraw-Hill (1981).
15. Y.C. Lin, Ming-Song Chen, Jue Zhong, Comp. Mat. Sci. **43**, 1117–1122 (2008).
16. Y.C Lin, Ming-Song Chen, Jue Zhong, J. Mat. Proc. Tech. **205**, 308–315 (2008).
17. Y.C. Lin, Chen X.M., Materials Design **32**, 1733–59 (2011).
18. Y.C. Lin, Liu Yan-Xing, Liu Ge, Chen Ming-Song, Huang Yuan-Chun, J. Mat. Eng. and Perf. **24**, 221–228 (2015).
19. Y.C. Lin, M. Chen M, J. Zhong, Materials Letters **62**, 2132–2135 (2008).
20. T.J. McCaffrey, Ultrahigh-strength steels. Metals handbook, ASM; 430(1990).
21. T. Miokovic, V. Schulze, O. Vohringer, D. Lohe, Mater Sci.Eng. A, 547–55 (2006).
22. A. Momeni, K. Dehghani, R. Ebrahimi, J. Alloy Compounds **509**, 9387–9393 (2011).
23. M. Nouari, A. Molinari, Wear **259**, 1151–1159 (2005).
24. M. Pop, D. Frunza, F. Popa, A. Neag, JOAM **17**(11-12), 1761–1766 (2015).
25. E. Rodriguez, M. Flores, A. Perez, R.D. Mercado-Solis, R. González, J. Rodríguez, Wear **267**, 2109–2115 (2009).
26. C.M.A. Silva, L.M. Alves, C.V. Nielsen, A.G. Atkins, P.A.F. Martins, J. Mat. Proc. Tech. **215**, 287–298 (2015).
27. P. Starke, F. Walther, D. Eifler, Mater. Sci. Eng. A **523**, 246–252 (2009).
28. C. Zener, J.H. Hollomon, J.Appl.Phys. **15,** 22–32 (1944).